



Cite this: *RSC Adv.*, 2017, 7, 19318

Promotional effect of lanthana on the high-temperature thermal stability of Pt/TiO₂ sulfur-resistant diesel oxidation catalysts†

Zhengzheng Yang,¹ Na Zhang,^a Yi Cao,^b Yunxiang Li,^a Yunwen Liao,^a Youping Li,^a Maochu Gong^{bc} and Yaoqiang Chen^{*bc}

In order to efficiently remove diesel exhaust pollutants during long-term application under high temperature conditions, enhancing the thermal stability of catalysts is essential. Here, lanthana was introduced into a TiO₂ sulfur-resistant support *via* co-precipitation, and then a Pt/TiO₂-La₂O₃ diesel oxidation catalyst (DOC) was prepared using the impregnation method. The SO₂ uptake and EDX results indicate that the La₂O₃-doped Pt/TiO₂-La₂O₃ catalyst displays superior sulfur resistance compared to the commercial Pt/Al₂O₃ and Pt-Pd/CeO₂-ZrO₂-Al₂O₃ DOC catalysts. Catalytic performance measurements showed that the as-prepared Pt/TiO₂-La₂O₃ catalyst exhibited significantly better activity than Pt/TiO₂ after high-temperature thermal aging and simulative 160 000 km vehicle aging. X-ray diffraction (XRD), X-ray photoelectron spectroscopy (XPS) and N₂ adsorption-desorption results suggest that some of the La³⁺ dopant ions migrated to the grain boundary of the TiO₂ crystal and other La³⁺ ions replaced Ti⁴⁺ ionic sites to form Ti-O-La bands, which impeded the crystal growth and phase transition of TiO₂, and hence mitigated the destruction of the porous texture of TiO₂. Transmission electron microscopy (TEM) and scanning electron microscopy (SEM) observations further demonstrate that the introduction of lanthana into TiO₂ suppressed Pt particle agglomeration and catalyst particle sintering, consequently enhancing the thermal stability of the Pt/TiO₂-La₂O₃ catalyst. Thus, this work shows that lanthana can play an extremely important role in improving the structural and textural stability of TiO₂ and stabilizing the surface-active component of the Pt/TiO₂ DOC catalyst, hence enhancing the high-temperature aging resistance.

Received 14th January 2017

Accepted 23rd March 2017

DOI: 10.1039/c7ra00582b

rsc.li/rsc-advances

1. Introduction

Diesel engines are widely applied due to their robustness and high fuel efficiency. However, hazardous substances from diesel exhausts such as carbon monoxide (CO), unburned hydrocarbons (HCs), various oxides of nitrogen (NO_x) and particulate matter (PM) must be effectively removed.^{1,2} In recent years, an integrated exhaust after-treatment system, containing a diesel oxidation catalyst (DOC) and a catalyzed diesel particulate filter with selective catalytic reduction, has been widely utilized for purifying diesel exhausts.^{3,4} The functions of the DOC in the after-treatment system are removing CO, HCs, and the soluble organic fraction (SOF), and oxidizing NO to NO₂.

Noteworthy, the sulfur poisoning resistibility of the DOC is a significant and non-ignorable element,⁵⁻⁷ because the sulfur content of commercial diesel fuels in developing countries is extremely high.^{8,9} Moreover, even with the introduction of ultra-low sulfur diesel (ULSD) fuels, sulfur poisoning still remains one of the most important factors impacting the reactivity of DOCs.^{10,11} This is because even with ULSD, SO₂ adsorption/condensation/desorption can still be a problem;¹² and current research¹⁰ implies that the amount of sulfur species accumulated on a DOC catalyst over its lifetime may amount to kilograms. Thus, studies on suppressing sulfur species accumulation on DOC catalysts and enhancing the sulfur poisoning resistibility of DOCs are practical and significant.¹²

To improve the sulfur tolerance of catalysts, TiO₂, as a non-sulfating material, has been introduced into vehicle exhaust catalysts and has played a commendable role.¹²⁻¹⁵ Furthermore, our previous studies¹⁶⁻¹⁸ have suggested that rare earth element doping can improve the activity and stability while maintaining the sulfur resistibility of TiO₂-based DOC catalysts. However, the anatase phase transition and decrease in specific surface area of TiO₂ under high temperatures^{19,20} result in platinum sintering and catalyst deactivation.¹² In the diesel exhaust after-treatment system, during active DPF regeneration, the DOC bed

^aCollege of Environmental Science and Engineering, China West Normal University, Nanchong 637009, Sichuan, China. E-mail: zyang@cwnu.edu.cn; Fax: +86 817 2568646; Tel: +86 817 2568646

^bKey Laboratory of Green Chemistry & Technology of the Ministry of Education, College of Chemistry, Sichuan University, Chengdu 610064, Sichuan, China. E-mail: nic7501@scu.edu.cn; Fax: +86 28 85418451; Tel: +86 28 85418451

^cSichuan Provincial Vehicular Exhaust Gases Abatement Engineering Technology Center, Chengdu 610064, Sichuan, China

† Electronic supplementary information (ESI) available. See DOI: 10.1039/c7ra00582b



temperature rises rapidly (and can reach up to 850 °C);^{11,21} additionally, diesel engines working at high loading or fast acceleration may also lead to a sharp rise in exhaust temperature. Thus, it is crucial for the thermal stability of TiO₂-based DOCs to be improved.

Research has proven that the addition of La can efficiently enhance the thermal stability of CeO₂ (ref. 22 and 23) and Al₂O₃.^{24,25} In addition, the performance of La-doped TiO₂ materials in photocatalytic reactions has been extensively investigated.^{26,27} Cong *et al.*²⁸ have recently reported that La³⁺ and N co-doping can enhance the thermal stability of TiO₂ microstructures and improve the photocatalytic activity of TiO₂. Moreover, Gopalan, Sibin and Reddy *et al.* have reported that lanthana doping is conducive to improving the phase and pore structure stability of TiO₂ at high temperature.^{29–31}

However, reports on the effects of lanthana on the porous textural features (*i.e.* specific surface area and pore volume) of TiO₂-based vehicular emission purification catalysts under high temperature are still scarce. Due to the fact that the porous texture of a vehicular emission purification catalyst is closely related to its catalytic performance,^{32,33} it is essential to improve the porous texture and high-temperature resistibility of TiO₂. Considering all of this, the effects of lanthana in enhancing the porous texture and high-temperature aging resistance of TiO₂-based sulfur-resistant diesel oxidation catalysts were investigated in this work.

2. Experimental

2.1 Materials

Ammonium hydroxide, TiOSO₄·2H₂O, and La(NO₃)₃·6H₂O were purchased from Chengdu Kelong Chemical Reagent Factory (China), (EA)₂Pt(OH)₆ solution (12.15% Pt w/w) was purchased from Heraeus, and all the chemicals were of analytical grade and used without further purification.

2.2 Catalyst synthesis

The TiO₂-La₂O₃ support was synthesized by co-precipitation with a molar ratio of Ti : La = 9 : 1, which is the optimal ratio according to our previous related work.^{17,18} The desired mixed solutions of TiOSO₄·2H₂O and La(NO₃)₃·6H₂O were slowly added into NH₃·H₂O solution under vigorous stirring, and then the precipitate was filtered and washed many times. After drying overnight and calcining at 500 °C for 3 h under airflow, the TiO₂-La₂O₃ support was obtained.

The Pt/TiO₂-La₂O₃ catalyst powder was prepared using the incipient impregnation method. (EA)₂Pt(OH)₆ solution was impregnated onto the TiO₂-La₂O₃ support with a Pt loading of 1.0 wt%. The resulting Pt/TiO₂-La₂O₃ powder was dried at 120 °C and calcined for 3 h at 500 °C in air, and then the catalyst powder was deposited onto a ceramic honeycomb (400 cells per square inch, 6 mill) with about 120 g L⁻¹ of washcoat loading, so as to prepare a monolithic catalyst. The monoliths obtained were dried at 120 °C overnight and calcined for 3 h at 500 °C in air. The Pt/TiO₂ catalyst was synthesized using the same method.

Commercial Pt/Al₂O₃ and Pt-Pd/CeO₂-ZrO₂-Al₂O₃ DOC catalysts were supplied by Sichuan provincial vehicular exhaust gases abatement engineering technology center.

The simulative 160 000 km vehicle-aged catalyst, labeled as Pt/TiO₂-La₂O₃(A), was prepared by following ref. 34. Fresh monolithic catalyst was placed in a reactor and aged at 670 °C for 15 h and then at 250 °C for 15 h in the following aging gases: 600 ppm C₃H₆, 1500 ppm CO, 200 ppm NO, 50 ppm SO₂, 5% O₂, 4% CO₂, 8% vapor, and N₂ balance at flow rate of 800 mL min⁻¹. The Pt/TiO₂(A), Pt/Al₂O₃(A) and Pt-Pd/CeO₂-ZrO₂-Al₂O₃(A) catalysts were obtained using the same method.

2.3 Catalytic performance measurements

The activities of the catalysts were tested on a multiple fixed bed continuous flow reactor. The monolith was placed in a quartz tube reactor with an electric heater. The simulative diesel exhaust gases³⁵ contained a mixture of 1000 ppm CO, 330 ppm C₃H₆, 200 ppm NO, 50 ppm SO₂, 8% CO₂, 7% vapor, 10% O₂, and N₂ balance at a gas space velocity of 60 000 h⁻¹, and were controlled by mass flow controllers.

The inlet gas temperature was measured by a K-thermocouple which was fixed 20 mm in front of the monolith to avoid the effect of oxidation reactions (exothermic). The catalyst bed temperature was measured by another 0.5 mm K-thermocouple which was placed in the middle of one of the center channels inside the monolith catalyst. The outlet CO was detected using an FGA-4100 automotive emission analyzer (Foshan Analytical Instrument Co., Ltd., China), and C₃H₆ was analyzed with a GC2000II online gas chromatograph (Shanghai Analysis Instruments, China) using a flame ionization detector (FID).

2.4 Catalyst characterization

SO₂ uptake testing was conducted as reported in ref. 36 and implemented on a HCT-2 (Henven Instruments, China) thermogravimetric analyzer (TGA). The samples (15 mg) were pre-treated in a 35 mL min⁻¹ flow of N₂ for 5 h at 300 °C. Then, a flow of 43 mL min⁻¹ SO₂(0.05 vol%)-N₂ and 31 mL min⁻¹ O₂(15.0 vol%)-N₂ was introduced at 300 °C for 4 h. The accumulation of sulfur species was defined as the percentage of mass gained.

CO chemisorption was performed in a quartz tube reactor at room temperature. About 0.15 g of sample was reduced in a hydrogen flow (H₂, 99.999%) of 50 mL min⁻¹ at 500 °C and exposed for 2 h. After cooling to room temperature in the same reducing stream, helium (He, 99.999%) was flowed through the sample for 10 min, and then the Pt dispersion of the sample was determined by CO chemisorption. Because both linearly bound and bridge-bound CO existed on the Pt catalyst, a factor of 0.8 CO/Pt was used to calculate the concentration of surface Pt atoms.³⁷

X-ray diffraction (XRD) patterns of the samples were obtained by power X-ray diffraction on a DX-1000 diffractometer (Dandong Fangyuan Instrument Co. Ltd., China) using Cu K α radiation.

X-ray photoelectron spectroscopy (XPS) data were acquired using a Kratos XSAM 800 spectrometer (Kratos Analytic Inc.)



with Al K α radiation, and the C 1s binding energy (BE, 284.8 eV) was used to calibrate the binding energy shifts of the samples.

Nitrogen adsorption–desorption isotherms were obtained on a QUADRASORB SI automated surface area and pore size analyzer (Quantachrome Instruments). The specific surface area and pore size were calculated using the BET and BJH method, respectively.

TEM images were acquired on a Tecnai G² F20 (E. A. Fischione Instruments Inc., USA) transmission electron microscope (TEM).

The surface morphologies of the catalysts were observed using a S-4800 (Hitachi Ltd.) scanning electron microscope (SEM), and the sulfur content of the aged catalysts was analyzed using an IE-250 (Oxford Instruments) energy dispersive X-ray (EDX) spectrometer.

3. Results and discussion

3.1 Sulfur resistibility

The sulfur resistibility of the catalysts was tested using SO₂ uptake testing. As shown in Fig. 1, following exposure to SO₂ and O₂, the weight of the as-prepared Pt/TiO₂ and Pt/TiO₂-

La₂O₃ catalyst samples increased with time; after about 3 h, the weight changing trend of the samples began to level-off. The final weight increments of the Pt/TiO₂ and Pt/TiO₂-La₂O₃ samples were about 1.80 wt% and 2.46 wt%, respectively. In the same SO₂ uptake experiment, the total weight increments of the current commercial Pt/Al₂O₃ and Pt-Pd/CeO₂-ZrO₂-Al₂O₃ DOC catalysts were about 5.66 wt% and 4.73 wt%, respectively. The normalized sulfur uptake was calculated using the following equation:³⁶

$$\text{Normalized sulfur uptake } (\mu\text{g m}^{-2}) = \frac{\text{sulfur content (wt\%)}}{100 \times \text{surface area (m}^2\text{)}}$$

where the surface area is the BET surface area of the sample.

The calculated results are listed in Table 1. The normalized sulfur uptakes of the Pt/TiO₂ and Pt/TiO₂-La₂O₃ samples were about 194 $\mu\text{g m}^{-2}$ and 191 $\mu\text{g m}^{-2}$, respectively; for the commercial Pt/Al₂O₃ and Pt-Pd/CeO₂-ZrO₂-Al₂O₃ DOC catalysts, the values were about 306 $\mu\text{g m}^{-2}$ and 230 $\mu\text{g m}^{-2}$, respectively. This indicates that compared with the current commercial Pt/Al₂O₃ and Pt-Pd/CeO₂-ZrO₂-Al₂O₃ DOC catalysts, the TiO₂-based catalysts (both Pt/TiO₂ and Pt/TiO₂-La₂O₃) did not heavily accumulate sulfur species, and hence the TiO₂-based catalysts displayed superior sulfur resistibility. This is because the non-sulfating material TiO₂ exhibits low SO₂ adsorption, and hence suppresses sulfate formation.^{12,38} Moreover, the doping of La into TiO₂ had essentially no effect on the naturally excellent sulfur resistance of the Pt/TiO₂ catalyst.

Meanwhile, according to the EDX testing results (Table 1), the amount of sulfur accumulated on the simulative 160 000 km vehicle-aged Pt/TiO₂(A) and Pt/TiO₂-La₂O₃(A) catalysts was about 1.34 wt% and 1.85 wt%, respectively, while the values for the commercial Pt/Al₂O₃(A) and Pt-Pd/CeO₂-ZrO₂-Al₂O₃(A) DOC catalysts were about 5.79 wt% and 4.40 wt%, respectively. The normalized sulfur uptake values calculated from the EDX results also showed the same trend, which implies that compared with the current commercial Pt/Al₂O₃ and Pt-Pd/CeO₂-ZrO₂-Al₂O₃ DOC catalysts, the as-prepared Pt/TiO₂ and Pt/TiO₂-La₂O₃ catalysts exhibit obviously reduced sulfur accumulation under long-term exposure to diesel exhaust conditions. Additionally, the catalytic activity measurements show that both the as-prepared Pt/TiO₂ and Pt/TiO₂-La₂O₃, and the commercial Pt/Al₂O₃ and Pt-Pd/CeO₂-ZrO₂-Al₂O₃ DOC catalysts displayed good purifying properties for diesel exhaust CO and C₃H₆; all the mentioned

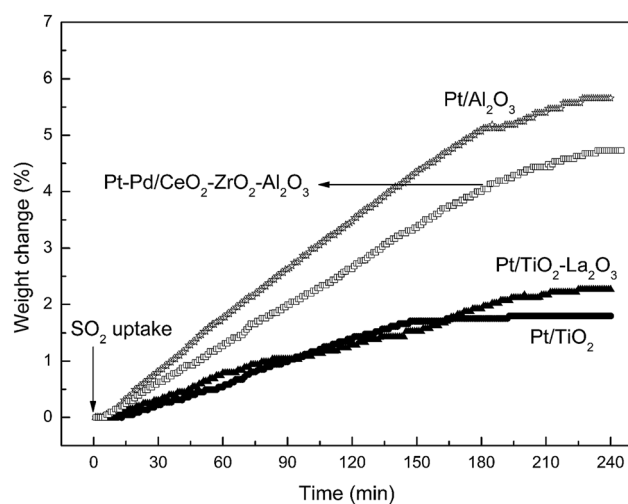


Fig. 1 SO₂ uptake of the as-prepared Pt/TiO₂ and Pt/TiO₂-La₂O₃, and commercial Pt/Al₂O₃ and Pt-Pd/CeO₂-ZrO₂-Al₂O₃ catalysts.

Table 1 Sulfur accumulation and normalized sulfur uptake over the Pt/TiO₂, Pt/TiO₂-La₂O₃, and commercial Pt/Al₂O₃ and Pt-Pd/CeO₂-ZrO₂-Al₂O₃ DOC catalysts

Sample	Surface area/(m ²)	Sulfur content (wt%)		Normalized sulfur uptake ($\mu\text{g m}^{-2}$)	
		SO ₂ uptake	EDX ^a	SO ₂ uptake	EDX ^a
Pt/TiO ₂	93	1.80	1.34	194	144
Pt/TiO ₂ -La ₂ O ₃	129	2.46	1.85	191	143
Pt/Al ₂ O ₃	185	5.66	5.79	306	313
Pt-Pd/CeO ₂ -ZrO ₂ -Al ₂ O ₃	206	4.73	4.40	230	214

^a EDX results were obtained by detecting the simulative 160 000 km vehicle-aged samples.



catalysts can completely purify diesel CO and C₃H₆ below 230 °C (ESI, Fig. 1†).

Because sulfur accumulation on catalysts leads to sulfur poisoning of the catalyst and hence activity degradation, our previous work verified that the commercial Pt/Al₂O₃ and Pt-Pd/CeO₂-ZrO₂-Al₂O₃ DOC catalysts were significantly deactivated due to the accumulation of sulfur on the catalyst surface, but the activity degradation of TiO₂-based catalysts resulting from sulfur poisoning was very slight.¹⁷ Thus, it can be suggested that compared to the current commercial Pt/Al₂O₃ and Pt-Pd/CeO₂-ZrO₂-Al₂O₃ DOC catalysts, the TiO₂-based catalysts (Pt/TiO₂ and Pt/TiO₂-La₂O₃) displayed superior sulfur resistibility, which is beneficial for maintaining catalytic activity during long-term use under SO₂-containing diesel exhaust conditions.

3.2 Catalytic activity and thermal stability

3.2.1 Effects of lanthana modification. Fig. 2 shows the catalytic activities of CO and C₃H₆ oxidation on the fresh and thermally aged Pt/TiO₂ and Pt/TiO₂-La₂O₃ catalysts. It can be seen that the catalytic performances of both the Pt/TiO₂ and Pt/TiO₂-La₂O₃ catalysts are decreased after 3 h of thermal treatment at 750 °C; however, modification with La significantly alleviated the reactivity decrease of the Pt/TiO₂-La₂O₃ catalyst. For the CO oxidation reaction (Fig. 2a), 3 h of thermal treatment at 750 °C lead to an 11 °C increase in the light-off temperature (*T*₅₀, the temperature when the conversion of the reactant reaches 50%) on the Pt/TiO₂ catalyst; the *T*₅₀ increment of the Pt/TiO₂-La₂O₃ catalyst resulting from aging at 750 °C is negligible (less than 2 °C). The same trend was also observed for the C₃H₆ combustion reaction (Fig. 2b), which demonstrates that La modification obviously mitigated the activity decrease of Pt/TiO₂ resulting from high-temperature treatment; that is, La doping can effectively enhance the thermo-stability of the Pt/TiO₂ catalyst.

Furthermore, the Pt/TiO₂-La₂O₃ catalyst shows significantly better catalytic performance than the Pt/TiO₂ catalyst, both after 3 h of thermal aging at 850 °C and after simulative 160 000 km vehicle aging (ESI, Fig. 2 and 3†). The CO and C₃H₆ *T*₅₀ values of Pt/TiO₂-La₂O₃(850), the sample treated at 850 °C for 3 h, are 221 °C and 236 °C, respectively; for Pt/TiO₂(850) the values are 232 °C and 240 °C, respectively (ESI, Fig. 2†). The 160 000 km vehicle-aged sample Pt/TiO₂-La₂O₃(A) shows CO and C₃H₆ light-off temperatures of 210 °C and 218 °C, respectively; the CO and C₃H₆ *T*₅₀ values of Pt/TiO₂(A) are 219 °C and 231 °C, respectively (ESI, Fig. 3†). It can be inferred that La doping results in an improvement in high-temperature resistance and long-term use durability. Additionally, it was proved that yttria-modified Pt/TiO₂-YO_x catalysts exhibited excellent low temperature activity and stability in our previous work,¹⁷ and the high-temperature resistibility of the Pt/TiO₂-YO_x catalyst was compared with that of the Pt/TiO₂-La₂O₃ catalyst (ESI, Fig. 4†). It can be seen that the Pt/TiO₂-YO_x catalyst showed the best low temperature activity for CO and C₃H₆ oxidation; however, after 3 h of thermal aging at 750 °C, the Pt/TiO₂-La₂O₃ catalyst displayed obviously better activity than Pt/TiO₂-YO_x, and after thermal aging at 850 °C for 3 h, Pt/TiO₂-La₂O₃ still exhibited better activity than

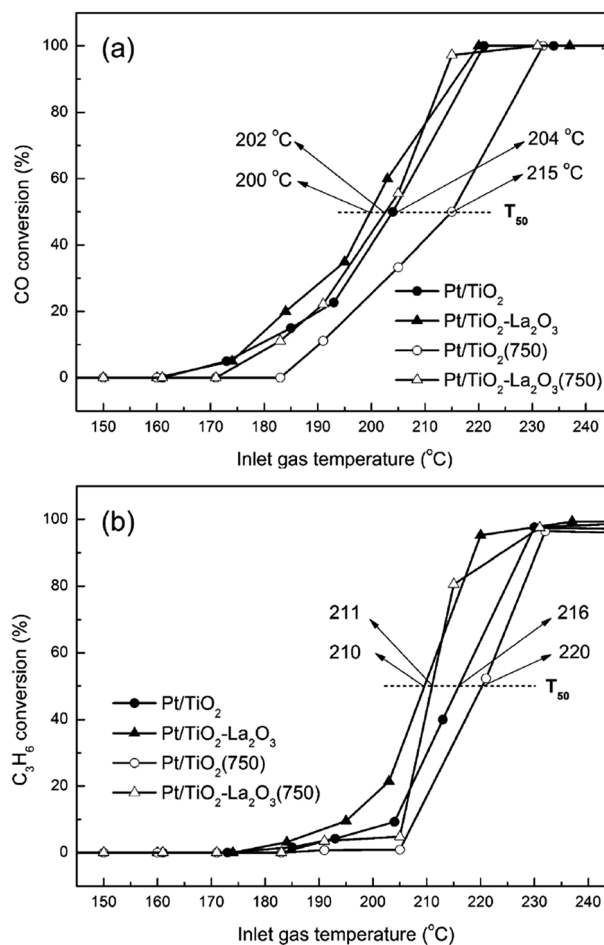


Fig. 2 The CO (a) and C₃H₆ (b) oxidation conversion over Pt/TiO₂, Pt/TiO₂-La₂O₃, Pt/TiO₂(750) and Pt/TiO₂-La₂O₃(750) catalysts. Reaction conditions: C₃H₆: 330 ppm, CO: 1000 ppm, NO: 200 ppm, O₂: 10%, CO₂: 8%, vapor: 7%, SO₂: 50 ppm, N₂: balance, GHSV = 60 000 h⁻¹. All catalysts were pre-treated at 500 °C for 3 h under the reaction atmosphere.

the Pt/TiO₂-YO_x catalyst. This suggests that the high-temperature resistibility of the lanthana-modified Pt/TiO₂-La₂O₃ catalyst is superior to that of the yttria-modified Pt/TiO₂ catalyst.

To clearly investigate the effects of La modification on the DOC reactivity after high-temperature treatment, the global reaction rates of both catalysts before and after 3 h of thermal treatment at 750 °C were determined. The calculated reaction rate results are listed in Table 2. It can be seen that the reaction rate of the Pt/TiO₂ catalyst for CO oxidation is 4.20×10^{-6} mol g⁻¹ s⁻¹, and the value reduces to 2.59×10^{-6} mol g⁻¹ s⁻¹ after thermal treatment at 750 °C for 3 h, which indicates that high-temperature treatment leads to a 40% reaction rate decrease of Pt/TiO₂ for CO oxidation. For the Pt/TiO₂-La₂O₃ catalyst, the catalytic activity decrease following the same thermal treatment could be ignored, because it was within the limit of measurement error (from 4.74×10^{-6} mol g⁻¹ s⁻¹ to 4.75×10^{-6} mol g⁻¹ s⁻¹). For C₃H₆ combustion, 3 h of high-temperature treatment at 750 °C resulted in a 43% decrease (from 6.09×10^{-7} mol g⁻¹ s⁻¹ to 3.49×10^{-7} mol g⁻¹ s⁻¹) in the



Table 2 CO and C₃H₆ reaction rates at 210 °C over the Pt/TiO₂, Pt/TiO₂-La₂O₃, Pt/TiO₂(750) and Pt/TiO₂-La₂O₃(750) catalysts

Catalyst	Reaction rate (mol g ⁻¹ s ⁻¹)	
	CO + O ₂	C ₃ H ₆ + O ₂
Pt/TiO ₂	4.20 × 10 ⁻⁶	6.09 × 10 ⁻⁷
Pt/TiO ₂ (750)	2.59 × 10 ⁻⁶	3.49 × 10 ⁻⁷
Pt/TiO ₂ -La ₂ O ₃	4.74 × 10 ⁻⁶	10.6 × 10 ⁻⁷
Pt/TiO ₂ -La ₂ O ₃ (750)	4.75 × 10 ⁻⁶	8.74 × 10 ⁻⁷

global reaction rate of the Pt/TiO₂ catalyst at 210 °C, while the decrease of the reaction rate of the Pt/TiO₂-La₂O₃ catalyst resulting from the high-temperature treatment is negligible (from 10.6 × 10⁻⁷ mol g⁻¹ s⁻¹ to 8.74 × 10⁻⁷ mol g⁻¹ s⁻¹). The activation energies of CO and C₃H₆ oxidation were not calculated because the presence of mixed gases (CO, C₃H₆, NO *etc.*) under simulative diesel exhaust conditions may affect the kinetic parameters of CO and C₃H₆ oxidation.^{17,39} Based on the above results, it can be suggested that the modification of the Pt/TiO₂ catalyst with La significantly mitigated the decrease in DOC reactivity resulting from high-temperature treatment, which in essence indicates that La doping can improve the thermo-stability of the Pt/TiO₂ catalyst.

3.2.2 Effects of high-temperature treatment. The relationship between the treatment temperature and the reaction rate at 210 °C for both of the catalysts is shown in Fig. 3. It is clear that the DOC reactivity of both the Pt/TiO₂ and Pt/TiO₂-La₂O₃ catalyst was not affected by 3 h of thermal treatment at 650 °C, which implies that the activity of both the catalysts could be maintained under the normal working conditions of a diesel engine. After thermal treated at 750 °C for 3 h, the CO and C₃H₆ catalytic performance of the Pt/TiO₂(750) catalyst was reduced by about 40% compared to the fresh Pt/TiO₂ catalyst, whereas the reactivity of Pt/TiO₂-La₂O₃(750) was almost not reduced; that is, an ultra-high exhaust temperature resulting from DPF regeneration or the diesel engine working under extreme conditions (such as ultra-high loading or fast acceleration *etc.*)

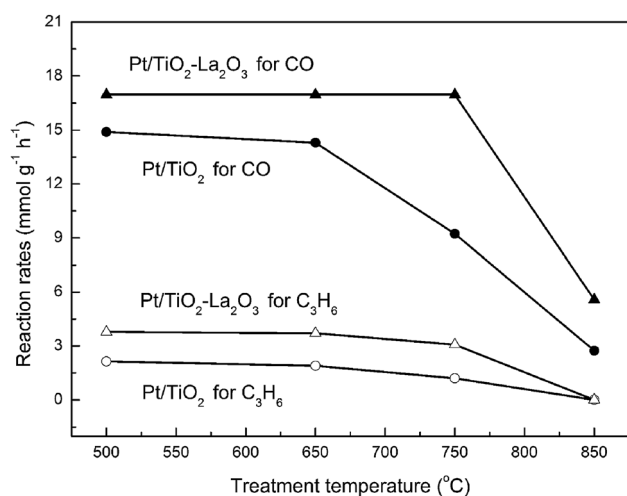


Fig. 3 CO and C₃H₆ reaction rates at 210 °C over the Pt/TiO₂ and Pt/TiO₂-La₂O₃ catalysts after 3 h of treatment at different temperatures.

would lead to the deactivation of the Pt/TiO₂ catalyst, but La doping can efficiently restrain the reactivity loss and enhance the thermal stability. The Pt/TiO₂-La₂O₃ catalyst was not obviously deactivated until the sample endured 3 h of baking at 850 °C. In order to investigate the effects of La in the Pt/TiO₂ catalyst, several characterization techniques were carried out.

3.3 Catalyst characterization

3.3.1 XRD analysis. Fig. 4 shows the XRD patterns of the TiO₂ and TiO₂-La₂O₃ supports at different temperatures. Typical anatase structure peaks are observed in the TiO₂ sample calcined at 500 °C, with a crystallite size of about 9.3 nm. As the temperature increased to 700 °C, a phase transition from anatase to rutile occurred; the ratio of rutile was about 14.3%, and the anatase crystallite size increased to 18 nm. When the temperature reaches 800 or 900 °C, the phase of TiO₂ is rutile with an average crystallite size of 33 or 39 nm. For all the La₂O₃-modified TiO₂ samples, no XRD characteristic peaks due to the crystalline La₂O₃ phase were observed; this observation indicates that La₂O₃ does not form complete crystals, and the La₂O₃ may be in a highly dispersed state or the La₂O₃ crystallites formed may be smaller than the detection ability of the XRD technique. TiO₂-La₂O₃ is mainly amorphous after calcining at 500 °C. Anatase structure peaks are observed in the TiO₂-La₂O₃ sample calcined at 700 °C, with a crystallite size of about 13 nm, and for the TiO₂-La₂O₃ sample calcined at 800 °C, the phase is still anatase with a crystallite size of 18 nm. The characteristic peaks of rutile are not observed until the temperature reaches up to 900 °C where the rutile characteristic peaks are weak, and the anatase crystallite size of the TiO₂-La₂O₃ sample calcined at 900 °C is about 30 nm. It can be seen that La₂O₃ modification retards the anatase-rutile phase transformation and postpones the crystal growth of TiO₂ under high temperature, thus stabilizing the structural properties of TiO₂. Moreover, the stabilization of the TiO₂ crystals by La₂O₃ is favorable for preventing the destruction of the texture of the TiO₂-based supports,^{19,20,40}

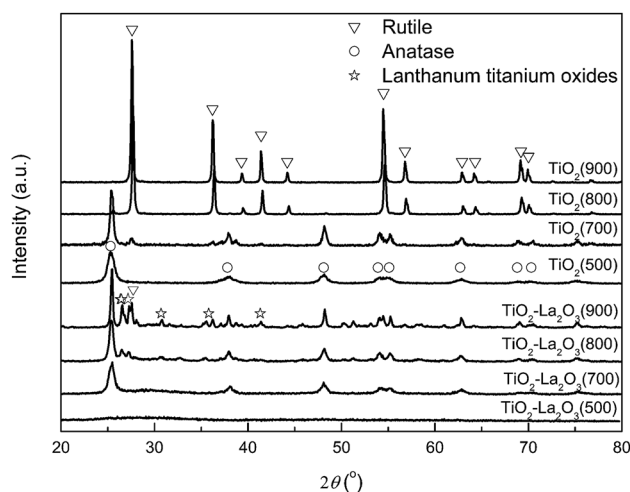


Fig. 4 XRD patterns of the TiO₂ and TiO₂-La₂O₃ supports after 3 h of treatment at different temperatures.



and enhancing the high-temperature resistance of the TiO₂-based catalyst.

Because the ionic radius of La³⁺ (0.1016 nm) is between that of Ti⁴⁺ (0.068 nm) and O²⁻ (0.132 nm),^{30,41} the La³⁺ ions should either replace the Ti⁴⁺ site or migrate to the grain boundary.³⁰ Thus, the stabilization of La₂O₃ in the TiO₂ crystal can be partly attributed to the segregation of lanthana dopant ions at the interstitial, which can inhibit the grain growth of TiO₂ by increasing the diffusion barrier at the titania–titania grain contacts and restricting the direct contact of the grains.^{30,42}

Besides the interstitial La₂O₃ segregation, the formation of Ti–O–La bands at the interface, resulting from some of the La³⁺ ions replacing some of the Ti⁴⁺ ionic sites, is another reason why La₂O₃ shows a stabilizing effect in TiO₂.^{28,43–45} Reddy, Siburu and Xu *et al.* have proven that Ti–O–La bands are formed in La₂O₃-doped TiO₂ mixed oxides.^{30,46,47} To further confirm the formation of Ti–O–La bands in the TiO₂–La₂O₃ compound in this work, XPS was employed.

3.3.2 XPS. The XPS spectra of the O 1s region of the as-prepared Pt/TiO₂ and Pt/TiO₂–La₂O₃ catalysts are provided in Fig. 5. Two peaks are observed for the Pt/TiO₂ sample; the peak with a binding energy of 530.0 eV is characteristic of lattice oxygen, and that with a binding energy of about 532.6 eV can be assigned to surface adsorbed oxygen.^{48–50} For the Pt/TiO₂–La₂O₃ catalyst, the characteristic peak of lattice oxygen is located at 529.7 eV, which is obviously shifted to a lower binding energy (decreasing by 0.3 eV); the peak for surface adsorbed oxygen is also located at 532.6 eV and the peak at 531.0 eV can be attributed to the contribution of chemisorbed oxygen or defect oxygen,^{49,50} which may result from the lattice oxygen separation of La₂O₃.^{51,52}

The XPS binding energy values of the Ti 2p_{3/2} and La 3d_{5/2} regions are listed in Table 3. The standard binding energy values of Ti 2p_{3/2} in TiO₂ and La 3d_{5/2} in La₂O₃ are 458.5 eV and 834.8 eV, respectively.⁵³ The binding energy of Ti in the Pt/TiO₂ catalyst is 458.5 eV, which is characteristic of TiO₂ (Ti⁴⁺) species, and this value is the same that for standard TiO₂. The binding energy of Ti in the Pt/TiO₂–La₂O₃ catalyst is 458.2 eV, which is

Table 3 Ti 2p and La 3d XPS parameters of the Pt/TiO₂ and Pt/TiO₂–La₂O₃ catalysts

Catalyst	Binding energy (eV)	
	Ti 2p _{3/2}	La 3d _{5/2}
Pt/TiO ₂	458.5	—
Pt/TiO ₂ –La ₂ O ₃	458.2	834.8
TiO ₂	458.5 (ref. 53)	—
La ₂ O ₃	—	834.9 (ref. 53)

obviously shifted to a lower energy than the value for standard TiO₂; this result indicates that some of the La³⁺ ions replace some of the Ti⁴⁺ sites and display a strong interaction with TiO₂. Meanwhile, the binding energy of La in the Pt/TiO₂–La₂O₃ catalyst is 834.8 eV, very close to the standard La₂O₃ value (834.9 eV), which suggests that in addition to the La³⁺ ions replacing the Ti⁴⁺ sites of TiO₂, a large number of La³⁺ ions in the Pt/TiO₂–La₂O₃ catalyst exist in the form of La₂O₃ species. These La₂O₃ species can act as a segregation agent in the TiO₂–La₂O₃ composite and hence inhibit TiO₂ grain growth by increasing the diffusion barrier and restricting the direct contact of the TiO₂–TiO₂ grains.^{30,42}

As presented in Fig. 5 and Table 3, in the Pt/TiO₂–La₂O₃ catalyst, the XPS characteristic binding energy values of both lattice oxygen (O²⁻) and Ti⁴⁺ are obviously shifted to lower binding energies, which can be attributed to the formation of Ti–O–La bands.⁴⁶ The formation of Ti–O–La bands provides a route for La³⁺ (which is more electropositive) to transfer electrons to O²⁻, and the increased concentration of electrons can be used to strengthen the bonding between the less electropositive Ti⁴⁺ ions.^{30,46} The increase in the electron density of O²⁻ and Ti⁴⁺ in the TiO₂–La₂O₃ composite results in the XPS binding energy shifting to lower values. Furthermore, the La³⁺ stabilized Ti–O bonds will in turn defer the phase transformation temperature of anatase-to-rutile, because the anatase-to-rutile phase transition requires the breaking of Ti–O bonds,³⁰ and the Ti–O bonds enhanced by La³⁺ ions are more difficult to break. Thus, the La₂O₃-stabilized TiO₂ exhibits superior high-temperature thermal stability.

3.3.3 Nitrogen adsorption–desorption. The stabilization of the structural properties of TiO₂ by La₂O₃ doping may enhance the textural stability of the TiO₂–La₂O₃ composite. To determine the texture of each catalyst support, the N₂ adsorption–desorption technique was used. As shown in Fig. 6, both the as-synthesized TiO₂(500) and TiO₂–La₂O₃(500) show distinct H3 and H4 complex hysteresis loops indicating slit pore features.^{54,55} When 3 h of thermal treatment at 700 °C was employed, some of the pores in both samples collapsed, but a distinct porous structure was still observed. After calcination at 800 °C for 3 h, which simulated high temperatures in a DOC bed resulting from active DPF regeneration, the TiO₂ support showed no obvious pore characteristics; however, the TiO₂–La₂O₃ support still showed a significant H3 hysteresis loop indicating slit pore features provided by schistous particles,^{54,55} until the temperature reached as high as 900 °C.

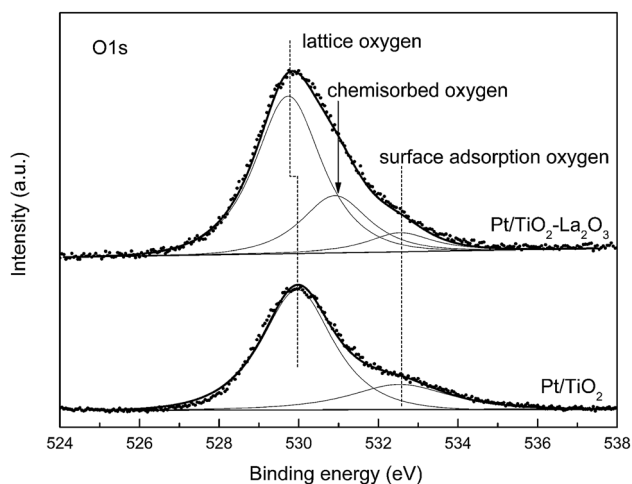


Fig. 5 XPS (O 1s) spectra of the Pt/TiO₂ and Pt/TiO₂–La₂O₃ catalysts.



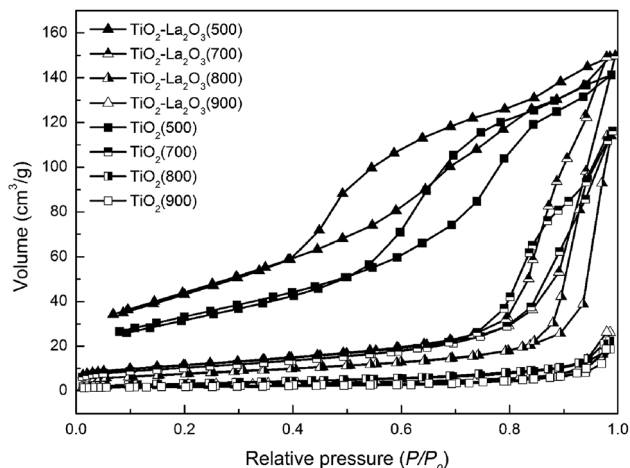


Fig. 6 Nitrogen adsorption-desorption isotherms of the TiO_2 and $\text{TiO}_2\text{-La}_2\text{O}_3$ supports after 3 h of treatment at different temperatures.

The calculated porous parameter results are listed in Table 4. The fresh $\text{TiO}_2(500)$ and $\text{TiO}_2\text{-La}_2\text{O}_3(500)$ supports show similar textural properties; the specific surface area of $\text{TiO}_2(500)$ is approximately $98 \text{ m}^2 \text{ g}^{-1}$ with an average pore volume of about $0.22 \text{ cm}^3 \text{ g}^{-1}$, and the specific surface area and average pore volume of $\text{TiO}_2\text{-La}_2\text{O}_3(500)$ are about $129 \text{ m}^2 \text{ g}^{-1}$ and $0.23 \text{ cm}^3 \text{ g}^{-1}$, respectively. Thermal treatment at $700 \text{ }^\circ\text{C}$ for 3 h led to a reduction in the surface area of both samples to near $40 \text{ m}^2 \text{ g}^{-1}$. When 3 h of thermal treatment at $800 \text{ }^\circ\text{C}$ was employed, the $\text{TiO}_2(800)$ sample lost its porous features, and the surface area and pore volume are just $11 \text{ m}^2 \text{ g}^{-1}$ and $0.03 \text{ cm}^3 \text{ g}^{-1}$, respectively. In contrast, the surface area of La doped- TiO_2 is more than $30 \text{ m}^2 \text{ g}^{-1}$, and in particular the pore volume of $\text{TiO}_2\text{-La}_2\text{O}_3(800)$, $0.18 \text{ cm}^3 \text{ g}^{-1}$, is similar to that of the fresh sample, which indicates that baking at $800 \text{ }^\circ\text{C}$ for 3 h did not obviously block the open pores and did not destroy the porous characteristics of the $\text{TiO}_2\text{-La}_2\text{O}_3$ support. As a result, the embedding of catalyst active components as a result of the texture of the support being destroyed is relieved. It is thus clear that La doping efficiently relieved the high-temperature sintering of TiO_2 , and maintained the good porous texture of the $\text{TiO}_2\text{-La}_2\text{O}_3$ support at high temperatures.

In order to further investigate the relationship between the structural properties and textural features of TiO_2 , the surface

Table 4 Textural properties of the TiO_2 and $\text{TiO}_2\text{-La}_2\text{O}_3$ supports after 3 h of treatment at different temperatures

Sample	Surface area ($\text{m}^2 \text{ g}^{-1}$)	Pore volume ($\text{cm}^3 \text{ g}^{-1}$)
$\text{TiO}_2(500)$	98	0.22
$\text{TiO}_2\text{-La}_2\text{O}_3(500)$	129	0.23
$\text{TiO}_2(700)$	36	0.18
$\text{TiO}_2\text{-La}_2\text{O}_3(700)$	40	0.23
$\text{TiO}_2(800)$	11	0.03
$\text{TiO}_2\text{-La}_2\text{O}_3(800)$	32	0.18
$\text{TiO}_2(900)$	7	0.03
$\text{TiO}_2\text{-La}_2\text{O}_3(900)$	9	0.04

area-crystallite size relationships of both supports after treatment at different temperatures were investigated as shown in Fig. 7. The crystallite size of amorphous $\text{TiO}_2\text{-La}_2\text{O}_3(500)$ was crudely estimated using the unsharp (101) crystal face of anatase, and the crystallite size of TiO_2 after calcining at $800 \text{ }^\circ\text{C}$ and $900 \text{ }^\circ\text{C}$ was calculated using the rutile crystal faces. It can be found that the surface area of both the TiO_2 and $\text{TiO}_2\text{-La}_2\text{O}_3$ supports declines and the crystallite size increases as the temperature rises. When the crystallite size is smaller than 20 nm , the surface area sharply declines with an increase in temperature; after that, when the crystallite size is larger than 20 nm , the changes in surface area and crystallite size with a rise in temperature tend to be moderate. Note that a surface area of no less than $30 \text{ m}^2 \text{ g}^{-1}$ is required to maintain the catalytic performance of vehicular emissions purification catalysts.^{32,56,57} The TiO_2 support exhibits a crystallite size of about 20 nm and a surface area of $30 \text{ m}^2 \text{ g}^{-1}$ at about $700 \text{ }^\circ\text{C}$, and the La-doped TiO_2 shows similar properties after 3 h of treatment at $800 \text{ }^\circ\text{C}$, which means that the TiO_2 -based catalyst can hardly maintain good activity at temperatures higher than $800 \text{ }^\circ\text{C}$, but the $\text{TiO}_2\text{-La}_2\text{O}_3$ catalyst can. That is, La modification can lead to TiO_2 -based DOCs that retain good reactivity at temperatures higher than $800 \text{ }^\circ\text{C}$ (the DOC bed temperature during active DPF regeneration). This corollary was confirmed by ESI Fig. 2.†

3.3.4 TEM. Catalyst supports with superior porous textures are advantageous for the dispersion of the active phase and hence improving the catalytic activity.⁵⁸⁻⁶⁰ The Pt particle sizes of the fresh and simulative vehicle-aged catalysts were observed by TEM. As presented in Fig. 8a and b, the Pt particles on the fresh Pt/TiO_2 and $\text{Pt/TiO}_2\text{-La}_2\text{O}_3$ catalysts are highly and homogeneously dispersed on the surface of the supports, and mimicking $160\,000 \text{ km}$ of vehicular exhaust aging obviously contributes to the Pt particle sintering of the $\text{Pt/TiO}_2(\text{A})$ (Fig. 8c) and $\text{Pt/TiO}_2\text{-La}_2\text{O}_3(\text{A})$ (Fig. 8d) catalysts. Based on the Pt particle size statistics obtained from the TEM images, the Pt particle size distributions of the catalysts were acquired and are displayed in Fig. 8e-h. For the Pt/TiO_2 catalyst (Fig. 8e), the Pt particle size

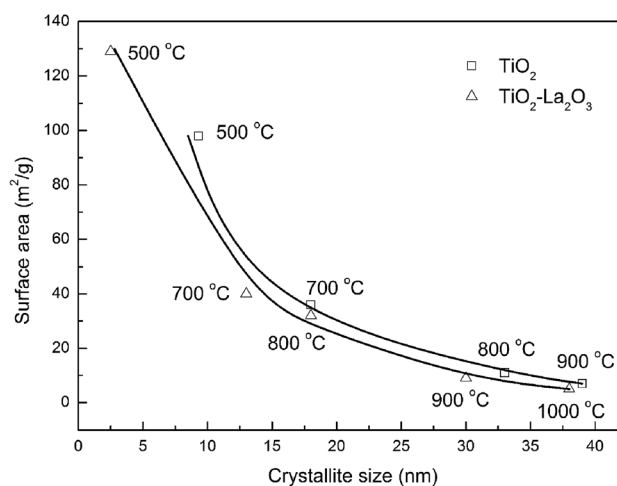


Fig. 7 The surface area-crystallite size relationships of the TiO_2 and $\text{TiO}_2\text{-La}_2\text{O}_3$ supports after 3 h of treatment at different temperatures.



distribution is between 0.73 nm and 3.28 nm with a mean size of 1.57 nm, estimated from over 300 particles from multiple TEM images. The Pt particle mean diameter of the Pt/TiO₂-

La₂O₃ catalyst (Fig. 8f) is about 1.39 nm and the size distribution is in the range of 0.65–3.25 nm (counting more than 300 Pt particles). To observe the Pt particles on the fresh catalysts more

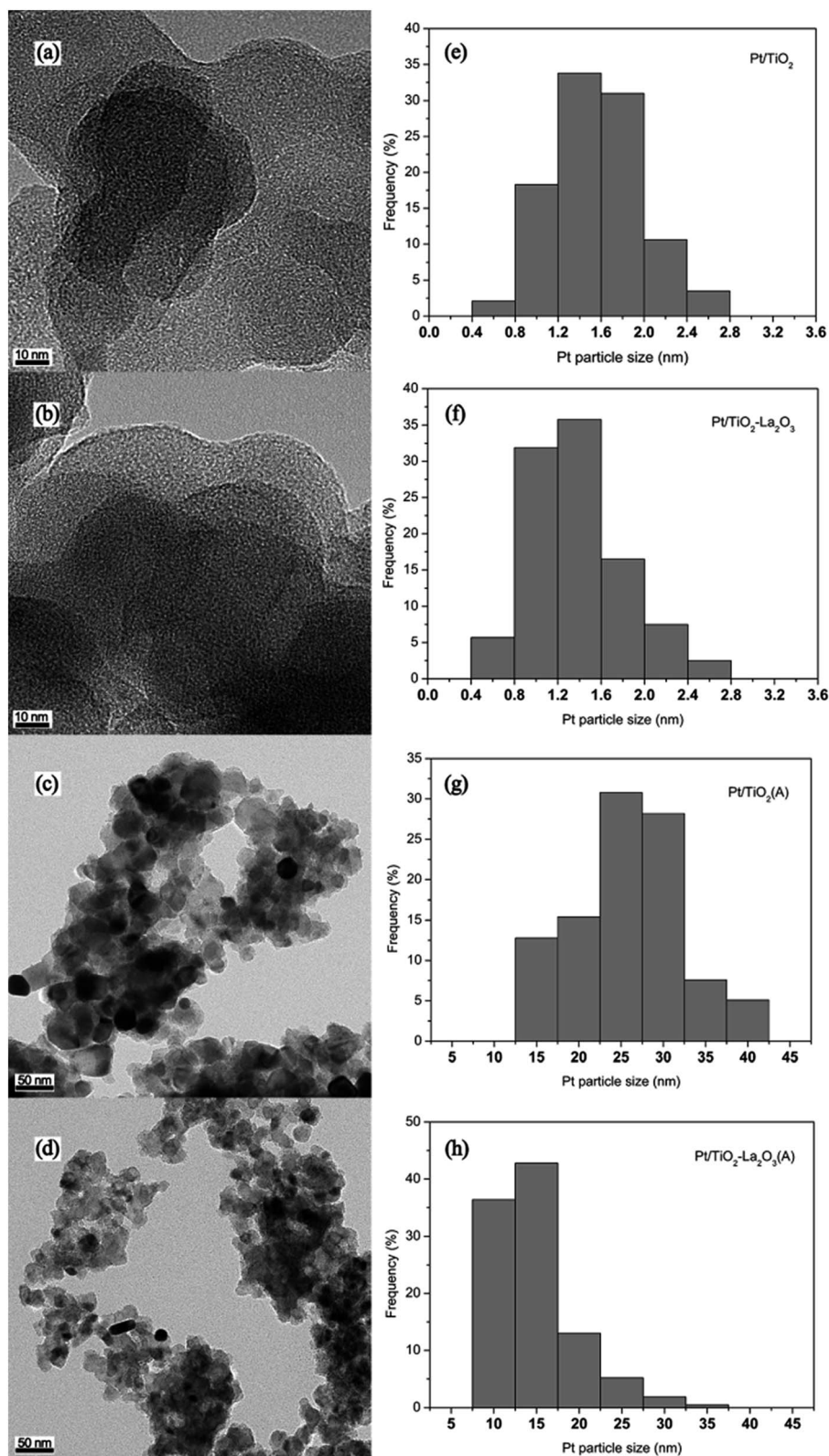


Fig. 8 TEM micrographs of the (a) Pt/TiO₂, (b) Pt/TiO₂-La₂O₃, (c) Pt/TiO₂(A), and (d) Pt/TiO₂-La₂O₃(A) catalysts, and (e-h) the related size distributions.

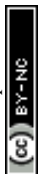


Table 5 Pt particle characteristics on the fresh and aged catalysts

Catalyst	Pt mean size (nm)	Pt surface area to volume ratio
Pt/TiO ₂	1.57	0.71
Pt/TiO ₂ -La ₂ O ₃	1.39	0.80
Pt/TiO ₂ (A)	25.90	0.043
Pt/TiO ₂ -La ₂ O ₃ (A)	14.78	0.076

Table 6 Pt surface concentration of the fresh and aged catalysts

Catalyst	Pt content (at%)
Pt/TiO ₂	0.87
Pt/TiO ₂ -La ₂ O ₃	0.73
Pt/TiO ₂ (A)	0.07
Pt/TiO ₂ -La ₂ O ₃ (A)	0.27

clearly, higher resolution TEM images were acquired and are supplied in Fig. 5 in the ESI.† For the aged catalysts, the mean Pt particle sizes of Pt/TiO₂(A) (Fig. 8g) and Pt/TiO₂-La₂O₃(A) (Fig. 8h) are 25.90 nm (in the range of 13.48 nm to 42.66 nm) and 14.78 nm (in the range of 8.26 nm to 36.42 nm), respectively, estimated from about 200 particles from multiple TEM images. Pt particles of smaller size have a better catalytic oxidation activity,^{61–63} due to the fact that smaller Pt particles supply a larger surface area to volume ratio and hence exhibit more surface Pt atoms (active phases).^{16,64} The Pt surface area to volume ratios of the as-prepared catalysts were estimated using the crude sphere model^{16,17} and are displayed in Table 5. It can be seen that the Pt surface area to volume ratio of Pt/TiO₂ is 0.72, which is roughly identical to the value (0.80) of the Pt/

TiO₂-La₂O₃ catalyst. However, the surface Pt atomic ratio of the aged Pt/TiO₂-La₂O₃(A) catalyst is about 0.076, which is almost twice as high as the surface Pt ratio (0.043) of the aged Pt/TiO₂(A) catalyst. It is thus clear that the Pt particles on both the Pt/TiO₂ and Pt/TiO₂-La₂O₃ catalysts are sintered into larger particles during the process of simulative 160 000 km vehicular exhaust aging, which is mainly caused by thermal sintering due to the high temperature of the exhaust gases. Compared to Pt/TiO₂, La-modified Pt/TiO₂-La₂O₃ can efficiently reduce Pt particle sintering and maintain a larger Pt surface area to volume ratio under exposure to high-temperature exhaust gases, and hence exhibit better catalytic performance after undergoing simulative 160 000 km vehicular exhaust aging, which is consistent with the results shown in ESI Fig. 3.†

3.3.5 SEM images and surface Pt concentration. In order to investigate whether La doping inhibited the sintering of TiO₂-based DOC catalysts during practical use, scanning electron microscopy (SEM) was employed to observe the catalyst morphologies before and after simulative 160 000 km vehicle aging. To get first-hand morphological information on the catalysts in practical use, ceramic honeycombs of the monolithic catalysts were cut and then were observed. As shown in Fig. 9, the Pt/TiO₂ catalyst exhibits an average particle size of about 2 μm with a few larger particles (5 μm), while for the Pt/TiO₂-La₂O₃ catalyst, the average particle size is about 4 μm with a few smaller particles (1–2 μm); after mimicking 160 000 km of vehicle aging, the particles size of the Pt/TiO₂(A) catalyst sharply increased to larger than 10 μm, while the Pt/TiO₂-La₂O₃(A) catalyst still exhibits a particle size of approximately 4 μm. Thus it can be seen that La modification successfully suppressed the sintering of the Pt/TiO₂ catalyst particles during long-term application under exposure to high-temperature diesel vehicular exhaust gases, which would reduce the embedding of

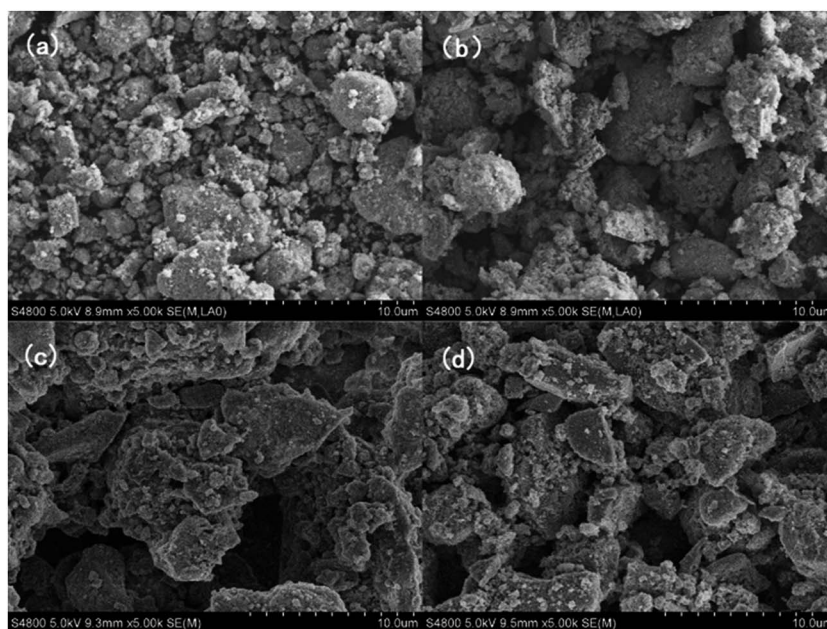


Fig. 9 SEM images of the fresh (a) Pt/TiO₂ and (b) Pt/TiO₂-La₂O₃ catalysts and the simulative vehicle-aged (c) Pt/TiO₂(A) and (d) Pt/TiO₂-La₂O₃(A) catalysts.



surface Pt species (active component) and hence mitigate the reactivity decrease.

To study the effect of catalyst particle sintering on the embedding of surface Pt particles, X-ray photoelectron spectroscopy (XPS) was carried out and the surface Pt atomic concentrations of the fresh and aged catalysts were estimated using the sensitivity factor method.⁵³ As shown in ESI Fig. 6,† the Pt (active phase) signal intensity for the fresh samples is obviously stronger than that for the mimicking vehicle-aged samples. The Pt chemical state differences between the fresh Pt/TiO₂ and Pt/TiO₂-La₂O₃ are potentially attributed to the difference in the Pt oxidation degree resulting from the difference in particle size.^{17,63} The surface Pt atomic concentrations of the catalysts are listed in Table 6; the surface Pt concentrations of fresh Pt/TiO₂ and Pt/TiO₂-La₂O₃ are 0.87 at% and 0.73 at%, respectively. For the simulative 160 000 km vehicle-aged samples, the surface Pt concentrations of Pt/TiO₂(A) and Pt/TiO₂-La₂O₃(A) are 0.07 at% and 0.27 at%, respectively. It can be seen that the surface Pt (active phase) content of the fresh catalysts is obviously higher than that of the mimicking vehicle-aged samples, mainly because of catalyst surface contamination and support pore structure collapse closing over the surface Pt particles during long-term use.^{34,65} In addition, the Pt dispersion of the fresh and 750 °C aged catalysts was measured by CO chemisorption. The Pt dispersions of Pt/TiO₂, Pt/TiO₂-La₂O₃, Pt/TiO₂(750) and Pt/TiO₂-La₂O₃(750) were 22.8%, 35.6%, 7.7% and 15.2%, respectively. It can be seen that after the same aging process, the surface Pt concentration of aged Pt/TiO₂-La₂O₃ is significantly higher than that of aged Pt/TiO₂, which indicates that there are significantly more exposed surface Pt species for aged Pt/TiO₂-La₂O₃ than for Pt/TiO₂. It is thus clear that La modification alleviated Pt/TiO₂-La₂O₃ catalyst surface active component loss during the aging process, and hence contributed to maintaining the excellent reactivity of Pt/TiO₂-La₂O₃ as well as improving the aging resistance. These analysis results show good agreement with the TEM results and catalytic activity results (ESI Fig. 3†).

4. Conclusions

From the above results, it can be concluded that an appropriate dopant amount of lanthana in TiO₂-La₂O₃ composites can maintain the naturally excellent sulfur resistance of TiO₂ and significantly enhance the high-temperature resistibility of TiO₂. Some of the La³⁺ doped ions migrate to the grain boundary of the TiO₂ crystal, which can inhibit the grain growth of TiO₂ by increasing the diffusion barrier at the TiO₂-TiO₂ grain contacts and restricting the direct contact of the grains. Other La³⁺ doped ions replace some of the Ti⁴⁺ ionic sites to form Ti-O-La bands at the interface. The formation of the La³⁺ stabilized Ti-O (Ti-O-La) bonds can defer the anatase-to-rutile phase transition temperature by causing the transfer of electrons from La³⁺ (which is more electropositive) to O²⁻, hence strengthening the bonding between the less electropositive Ti⁴⁺ ions. The stabilization of the TiO₂ crystal structure by the La³⁺ dopant is favorable for maintaining the good texture of the TiO₂-La₂O₃ composite at high temperatures, and consequently restraining

Pt particle agglomeration and surface Pt atom loss. Furthermore, the stabilization of the TiO₂-La₂O₃ texture is beneficial for suppressing the catalyst particle sintering of Pt/TiO₂-La₂O₃ at high temperatures, meaning that the as-prepared Pt/TiO₂-La₂O₃ catalyst still exhibits superior activity even after different high-temperature aging processes. The catalytic performance of the La₂O₃-modified Pt/TiO₂-La₂O₃ catalyst for the purification of diesel exhaust gases (CO and C₃H₆) is almost not reduced after thermal treatment at 750 °C; however, the reactivity of the Pt/TiO₂ catalyst is reduced by about 40% after the 750 °C treatment. Additionally, the 850 °C thermally treated catalysts and simulative 160 000 km vehicle-aged samples also show the same trend; lanthana modification obviously enhanced the high-temperature resistance of the Pt/TiO₂ catalyst. Thus, this work demonstrates that lanthana-modified Pt/TiO₂-La₂O₃ DOC catalysts display excellent high-temperature thermal stability and efficiently maintain the naturally outstanding sulfur resistance of TiO₂-based catalysts, which is beneficial for practical applications.

Acknowledgements

This work was supported by the Doctor Startup Foundation of China West Normal University (15E012), Natural Science Foundation of Science and Technology Department of Sichuan Province (2012FZ0008), National Natural Science Foundation of China (21173153), and National High-Tech Research and Development Program of China (863) (2013AA065304). The authors gratefully acknowledge Dr Wei Hu (College of Chemical Engineering, Sichuan University) and Ms Yufen Huang (College of Chemistry, Sichuan University) for providing CO chemisorption analysis and testing the activity of the catalysts.

References

- 1 D. Fino, S. Bensaid, M. Piumetti and N. Russo, A review on the catalytic combustion of soot in Diesel particulate filters for automotive applications: From powder catalysts to structured reactors, *Appl. Catal., A*, 2016, **509**, 75–96.
- 2 C. Liu, J.-W. Shi, C. Gao and C. Niu, Manganese oxide-based catalysts for low-temperature selective catalytic reduction of NO_x with NH₃: A review, *Appl. Catal., A*, 2016, **522**, 54–69.
- 3 T. Johnson, *Review of Vehicular Emissions Trends*, SAE Technical Paper, 2015-01-0993, 2015.
- 4 T. Johnson, *Vehicular Emissions in Review*, SAE Technical Paper, 2014-01-1491, 2014.
- 5 A. K. Wu, X. D. Yang, H. Zhou and K. J. Lu, Applied Mechanics and Materials, *Study on the Effect of Fuel Sulfur Content on Emission Characteristics in Diesel Engine*, Trans Tech Publ, 2014, pp. 27–30.
- 6 Z.-Z. Yang, Y. Yang, M. Zhao, M.-C. Gong and Y.-Q. Chen, Enhanced Sulfur Resistance of Pt-Pd/CeO₂-ZrO₂-Al₂O₃ Commercial Diesel Oxidation Catalyst by SiO₂ Surface Cladding, *Acta Phys.-Chim. Sin.*, 2014, **30**, 1187–1193.
- 7 H. N. Sharma, S. L. Suib and A. B. Mhadeshwar, Interactions of Sulfur Oxides with Diesel Oxidation Catalysts (DOCs),



- Novel Materials for Catalysis and Fuels Processing*, Oxford University Press, USA, 2013, vol. 1132, pp. 117–155.
- 8 K. Zhang, J. Hu, S. Gao, Y. Liu, X. Huang and X. Bao, Sulfur content of gasoline and diesel fuels in northern China, *Energy Policy*, 2010, **38**, 2934–2940.
 - 9 P.-Q. Tan, Z.-Y. Hu and D.-M. Lou, Regulated and unregulated emissions from a light-duty diesel engine with different sulfur content fuels, *Fuel*, 2009, **88**, 1086–1091.
 - 10 J. Li, A. Kumar, X. Chen, N. Currier and A. Yezerets, *Impact of Different Forms of Sulfur Poisoning on Diesel Oxidation Catalyst Performance*, SAE Technical Paper, 2013-01-0514, 2013.
 - 11 J.-Y. Luo, D. Kisinger, A. Abedi and W. S. Epling, Sulfur release from a model Pt/Al₂O₃ diesel oxidation catalyst: Temperature-programmed and step-response techniques characterization, *Appl. Catal., A*, 2010, **383**, 182–191.
 - 12 Y. Kanno, T. Hihara, T. Watanabe and K. Katoh, *Low Sulfate Generation Diesel Oxidation Catalyst*, SAE Technical Paper, 2004-01-1427, 2004.
 - 13 J. Li, Y. Zhu, R. Ke and J. Hao, Improvement of catalytic activity and sulfur-resistance of Ag/TiO₂-Al₂O₃ for NO reduction with propene under lean burn conditions, *Appl. Catal., B*, 2008, **80**, 202–213.
 - 14 H. Hirata, I. Hachisuka, Y. Ikeda, S. Tsuji and S. i. Matsumoto, NO_x storage-reduction three-way catalyst with improved sulfur tolerance, *Top. Catal.*, 2001, **16**, 145–149.
 - 15 U. Hideaki, *Development of Catalyst for Diesel Engine*, SAE Technical Paper, 980195, 1998.
 - 16 Z. Yang, J. Li, H. Zhang, Y. Yang, M. Gong and Y. Chen, Size-dependent CO and propylene oxidation activities of platinum nanoparticles on the monolithic Pt/TiO₂-YO_x diesel oxidation catalyst under simulative diesel exhaust conditions, *Catal. Sci. Technol.*, 2015, **5**, 2358–2365.
 - 17 Z. Yang, N. Zhang, Y. Cao, M. Gong, M. Zhao and Y. Chen, Effect of yttria in Pt/TiO₂ on sulfur resistance diesel oxidation catalysts: enhancement of low-temperature activity and stability, *Catal. Sci. Technol.*, 2014, **4**, 3032–3043.
 - 18 Z. Yang, Y. Chen, M. Zhao, J. Zhou, M. Gong and Y. Chen, Preparation and Properties of Pt/Zr_xTi_{1-x}O₂ Catalysts with Low-Level SO₂ Oxidation Activity for Diesel Oxidation, *Chin. J. Catal.*, 2012, **33**, 819–826.
 - 19 J. Yang, S. Mei and J. M. Ferreira, Hydrothermal synthesis of nanosized titania powders: influence of peptization and peptizing agents on the crystalline phases and phase transitions, *J. Am. Ceram. Soc.*, 2000, **83**, 1361–1368.
 - 20 J. F. Porter, Y.-G. Li and C. K. Chan, The effect of calcination on the microstructural characteristics and photoreactivity of Degussa P-25 TiO₂, *J. Mater. Sci.*, 1999, **34**, 1523–1531.
 - 21 G. Cavataio, H.-W. Jen, J. W. Girard, D. Dobson, J. R. Warner and C. K. Lambert, *Impact and prevention of ultra-low contamination of platinum group metals on SCR catalysts due to DOC design*, SAE Technical Paper, 2009-01-0627, 2009.
 - 22 A. Bueno-López, I. Such-Basáñez and C. Salinas-Martínez de Lecea, Stabilization of active Rh₂O₃ species for catalytic decomposition of N₂O on La-, Pr-doped CeO₂, *J. Catal.*, 2006, **244**, 102–112.
 - 23 P. Jiang, G. Lu, Y. Li, Y. Guo, Y. Guo and X. Wang, Preparation of La₂O₃-doped CeO₂-ZrO₂ Solid Solution with High Thermal Stability by Water-in-Oil Microemulsion, *Chem. Lett.*, 2004, **33**, 1064–1065.
 - 24 R. Strobel, S. E. Pratsinis and A. Baiker, Flame-made Pd/La₂O₃/Al₂O₃ nanoparticles: thermal stability and catalytic behavior in methane combustion, *J. Mater. Chem.*, 2005, **15**, 605–610.
 - 25 T. Yamamoto, T. Hatsui, T. Matsuyama, T. Tanaka and T. Funabiki, Structures and Acid-Base Properties of La/Al₂O₃ Role of La Addition to Enhance Thermal Stability of γ-Al₂O₃, *Chem. Mater.*, 2003, **15**, 4830–4840.
 - 26 Y.-T. Ma and S.-D. Li, Photocatalytic Activity of TiO₂ Nanofibers with Doped La Prepared by Electrospinning Method, *J. Chin. Chem. Soc.*, 2015, **62**, 380–384.
 - 27 X.-M. Chen, Z.-J. Liu, J.-T. Tang, C.-L. Teng, T.-J. Cai and Q. Deng, La-modified mesoporous TiO₂ nanoparticles with enhanced photocatalytic activity for elimination of VOCs, *J. Porous Mater.*, 2015, **22**, 361–367.
 - 28 Y. Cong, B. Tian and J. Zhang, Improving the thermal stability and photocatalytic activity of nanosized titanium dioxide via La³⁺ and N co-doping, *Appl. Catal., B*, 2011, **101**, 376–381.
 - 29 R. Gopalan and Y. S. Lin, Evolution of Pore and Phase Structure of Sol-Gel Derived Lanthana Doped Titania at High Temperatures, *Ind. Eng. Chem. Res.*, 1995, **34**, 1189–1195.
 - 30 C. P. Sibu, S. R. Kumar, P. Mukundan and K. G. K. Warriar, Structural Modifications and Associated Properties of Lanthanum Oxide Doped Sol-Gel Nanosized Titanium Oxide, *Chem. Mater.*, 2002, **14**, 2876–2881.
 - 31 B. M. Reddy, P. M. Sreekanth, E. P. Reddy, Y. Yamada, Q. Xu, H. Sakurai and T. Kobayashi, Surface Characterization of La₂O₃-TiO₂ and V₂O₅/La₂O₃-TiO₂ Catalysts, *J. Phys. Chem. B*, 2002, **106**, 5695–5700.
 - 32 M. Aubert, T. Birchem and G. Blanchard, Composition based on cerium oxide and on zirconium oxide with a high specific surface and a high oxygen storage capacity, process of preparation and use in catalysts, *US Pat.*, 6,228,799, 2001.
 - 33 O. Larcher and E. Rohart, Composition based on cerium oxide and on zirconium oxide having a high reducibility and high specific surface, methods for the preparation thereof and use as a catalyst, *US Pat.*, 8,192,710, 2012.
 - 34 J. Andersson, M. Antonsson, L. Eurenus, E. Olsson and M. Skoglundh, Deactivation of diesel oxidation catalysts: Vehicle- and synthetic aging correlations, *Appl. Catal., B*, 2007, **72**, 71–81.
 - 35 J. Kašpar, P. Fornasiero and N. Hickey, Automotive catalytic converters: current status and some perspectives, *Catal. Today*, 2003, **77**, 419–449.
 - 36 M. M. Koranne and J. N. Pryor, Sulfur tolerant alumina catalyst support, *US Pat.*, 8158257, 2012.
 - 37 K. Fogger and J. R. Anderson, Temperature programmed desorption of carbon monoxide adsorbed on supported platinum catalysts, *Appl. Surf. Sci.*, 1979, **2**, 335–351.



- 38 H. Ueno, T. Furutani, T. Nagami, N. Aono, H. Goshima and K. Kasahara, *Development of catalyst for diesel engine*, SAE Technical Paper, 980195, 1998.
- 39 S. E. Voltz, C. R. Morgan, D. Liederman and S. M. Jacob, Kinetic Study of Carbon Monoxide and Propylene Oxidation on Platinum Catalysts, *Ind. Eng. Chem. Prod. Res. Dev.*, 1973, **12**, 294–301.
- 40 J. M. G. Amores and V. S. Escribano, Anatase crystal growth and phase transformation to rutile in high-area TiO₂, MoO₃-TiO₂ and other TiO₂-supported oxide catalytic systems, *J. Mater. Chem.*, 1995, **5**, 1245–1249.
- 41 R. C. Weast and M. J. Astle, *Handbook of Chemistry and Physics*, CRC Press, Boca Raton, FL, 59th edn, 1978.
- 42 X.-Z. Ding and X.-H. Liu, Correlation Between Anatase-to-rutile Transformation and Grain Growth in Nanocrystalline Titania Powders, *J. Mater. Res.*, 1998, **13**, 2556–2559.
- 43 X. Quan, H. Tan, Q. Zhao and X. Sang, Preparation of lanthanum-doped TiO₂ photocatalysts by coprecipitation, *J. Mater. Sci.*, 2007, **42**, 6287–6296.
- 44 K. M. Parida and N. Sahu, Visible light induced photocatalytic activity of rare earth titania nanocomposites, *J. Mol. Catal. A: Chem.*, 2008, **287**, 151–158.
- 45 K. B. Jaimy, S. Ghosh and K. Gopakumar Warriar, Enhanced visible light activity of nano-titanium dioxide doped with multiple ions: Effect of crystal defects, *J. Solid State Chem.*, 2012, **196**, 465–470.
- 46 B. M. Reddy, B. Chowdhury and P. G. Smirniotis, An XPS study of La₂O₃ and In₂O₃ influence on the physicochemical properties of MoO₃/TiO₂ catalysts, *Appl. Catal., A*, 2001, **219**, 53–60.
- 47 D. Xu, L. Feng and A. Lei, Characterizations of lanthanum trivalent ions/TiO₂ nanopowders catalysis prepared by plasma spray, *J. Colloid Interface Sci.*, 2009, **329**, 395–403.
- 48 D. R. Sellick, A. Aranda, T. García, J. M. López, B. Solsona, A. M. Mastral, D. J. Morgan, A. F. Carley and S. H. Taylor, Influence of the preparation method on the activity of ceria zirconia mixed oxides for naphthalene total oxidation, *Appl. Catal., B*, 2013, **132–133**, 98–106.
- 49 Y. Yang, Z.-Z. Yang, H.-D. Xu, B.-Q. Xu, Y.-H. Zhang, M.-C. Gong and Y.-Q. Chen, Influence of La on CeO₂-ZrO₂ Catalyst for Oxidation of Soluble Organic Fraction from Diesel Exhaust, *Acta Phys.-Chim. Sin.*, 2015, **31**, 2358–2365.
- 50 A. Galtayries, R. Sporcken, J. Riga, G. Blanchard and R. Caudano, XPS comparative study of ceria/zirconia mixed oxides: powders and thin film characterisation, *J. Electron Spectrosc. Relat. Phenom.*, 1998, **88–91**, 951–956.
- 51 Z. Nie, T. Zuo, M. Zhou, Y. Wang, J. Wang and J. Zhang, High Temperature XPS/AES Investigation of Mo-La₂O₃ Cathode I. Species and Properties of Oxygen on Surface, *J. Chin. Soc. Rare Earths*, 1999, **17**, 135–139.
- 52 J. Wang, Z. Nie, M. Zhou, J. Zhang, Y. Hu and T. Zuo, A Study of Chemical Stability of La₂O₃ in Carburized La₂O₃-Mo Cathode Materials, *Chin. Rare Earths*, 2000, **21**, 18–21.
- 53 C. D. Wagner, W. M. Riggs, J. F. Moulder and G. E. Muilenberg, *Handbook of X-Ray Photoelectron Spectroscopy*, Perkin-Elmer Corporation, Minnesota, 1979.
- 54 M. Thommes, Physical adsorption characterization of nanoporous materials, *Chem.-Ing.-Tech.*, 2010, **82**, 1059–1073.
- 55 G. Leofanti, M. Padovan, G. Tozzola and B. Venturelli, Surface area and pore texture of catalysts, *Catal. Today*, 1998, **41**, 207–219.
- 56 M. Aubert, T. Birchem, G. Blanchard and O. Touret, Composition based on zirconium oxide and cerium oxide, preparation method therefor and use thereof, *US Pat.*, 6,214,306, 2001.
- 57 C. Hedouin, Process for preparing an oxide based on zirconium and titanium, oxides obtained thereby, and use of said oxides as catalysts, *US Pat.*, 7,524,474, 2009.
- 58 J. A. Hunns, M. Arroyo, A. F. Lee, J. M. Escola, D. Serrano and K. Wilson, Hierarchical mesoporous Pd/ZSM-5 for the selective catalytic hydrodeoxygenation of *m*-cresol to methylcyclohexane, *Catal. Sci. Technol.*, 2016, **6**, 2560–2564.
- 59 P. S. F. Mendes, G. Lapisardi, C. Bouchy, M. Rivallan, J. M. Silva and M. F. Ribeiro, Hydrogenating activity of Pt/zeolite catalysts focusing acid support and metal dispersion influence, *Appl. Catal., A*, 2015, **504**, 17–28.
- 60 T. Wu, Q. Zhang, W. Cai, P. Zhang, X. Song, Z. Sun and L. Gao, Phyllosilicate evolved hierarchical Ni- and Cu-Ni/SiO₂ nanocomposites for methane dry reforming catalysis, *Appl. Catal., A*, 2015, **503**, 94–102.
- 61 R. Portela, V. E. Garcia-Sanchez, M. Villarroel, S. B. Rasmussen and P. Avila, Influence of the pore generation method on the metal dispersion and oxidation activity of supported Pt in monolithic catalysts, *Appl. Catal., A*, 2016, **510**, 49–56.
- 62 C. Chen, F. Chen, L. Zhang, S. Pan, C. Bian, X. Zheng, X. Meng and F.-S. Xiao, Importance of platinum particle size for complete oxidation of toluene over Pt/ZSM-5 catalysts, *Chem. Commun.*, 2015, **51**, 5936–5938.
- 63 A. Boubnov, S. Dahl, E. Johnson, A. P. Molina, S. B. Simonsen, F. M. Cano, S. Helveg, L. J. Lemus-Yegres and J.-D. Grunwaldt, Structure-activity relationships of Pt/Al₂O₃ catalysts for CO and NO oxidation at diesel exhaust conditions, *Appl. Catal., B*, 2012, **126**, 315–325.
- 64 S. Bonanni, K. Ait-Mansour, W. Harbich and H. Brune, Reaction-Induced Cluster Ripening and Initial Size-Dependent Reaction Rates for CO Oxidation on Pt_n/TiO₂(110)-(1x1), *J. Am. Chem. Soc.*, 2014, **136**, 8702–8707.
- 65 A. Winkler, D. Ferri and M. Aguirre, The influence of chemical and thermal aging on the catalytic activity of a monolithic diesel oxidation catalyst, *Appl. Catal., B*, 2009, **93**, 177–184.

